Electronic Supplementary Information for CC-COM-04-2012-032886

Stabilisation of a Triply-Bridging Cyclopentadienyl Ligand in a Tetrapalladium Cluster

Kirill Yu. Monakhov,[†] *Christophe Gourlaouen,*[‡] *and Pierre Braunstein**[,†]

† Laboratoire de Chimie de Coordination, Institut de Chimie (UMR 7177 CNRS), Université de Strasbourg, 4 rue Blaise Pascal, CS 90032, F-67081 Strasbourg Cedex, France. E-mail: braunstein@unistra.fr; Fax: +33 (0)3 68 85 13 22; Tel: *+33 (0)3 68 85 13 08.*

‡ Laboratoire de Chimie Quantique, Institut de Chimie (UMR 7177 CNRS), Université de Strasbourg, 1 rue Blaise Pascal, BP 296/R8, F-67008 Strasbourg Cedex, France.

Contents

I. Experimental Section

1. General methods

All manipulations were carried out with the use of standard Schlenk techniques under an argon atmosphere. All organic solvents were distilled, dried and degassed according to standard procedures. NaCp was prepared according to a standard procedure.[1] Elemental analyses were performed in the Microanalytical Laboratory of the "Institut de Chimie, Strasbourg". ^{1}H NMR spectra were recorded with an FT Bruker Advance-300 instrument (^{1}H: 300.0 MHz). Chemical shifts are reported in δ units (ppm) and are referenced to external standard of tetramethylsilane (TMS) $SiMe_4$ as δ 0.00. The IR spectrum of **1**·0.5Et_2O in the solid state was recorded from 4000 to 600 cm^{-1} with a Thermo-Nicolet 6700 spectrometer, equipped with a diamond crystal SMART ORBIT accessory.

2. Synthesis of complex **1**·0.5Et_2O

The solution of NaCp (0.185 g, 2.1 mmol) in 15 mL of THF was added dropwise to a stirred solution of [$Pd(OAc)_2$] (0.224 g, 1.0 mmol) in 20 mL of THF at –78 °C. The reaction mixture was stirred for 6 h at low temperature and was then slowly warmed to ambient temperature to give a dark-red mixture. All volatiles were removed under reduced pressure. The residue was extracted twice with 20 mL of CH_2Cl_2. The volume of the CH_2Cl_2 solution was reduced to *ca*. 2 mL, and the solution was layered with 5 mL of Et_2O and placed at –20 °C. Black crystals of **1**·0.5Et_2O suitable for the X-ray diffraction were obtained. Yield: 0.105 g (53% based on Pd). Complex **1** is poorly soluble in usual NMR solvents. Anal. Found: C, 29.02%; H, 3.54%. Calcd. for $C_{18}H_{22}O_8Pd_4$·0.5Et_2O: C, 28.96%; H, 3.26%. ^{1}H NMR (300 MHz, C_6D_6): δ = 1.38 (s, CH_3), 1.53 (s, CH_3), 1.81 (s, CH_3), 1.91 (s, CH_3), 3.26 (m, 1H of η^1-(μ_3)-C_5H_5), 4.69, 4.97, 5.08, 5.51 (m, 1H each of η^2-(μ_3)-C_5H_5), 6.08 (s, η^5-C_5H_5). IR (cm^{-1}): $\tilde{\nu}$ = 3100 w, 3080 w, 2962 w, 2927w, 2855 w, 1596 m, 1535 m, 1396 m, 1339 m, 1287 w, 1258 s, 1082 s, 1008 s, 942 w, 860 w, 791 s, 683 s, 622 w.

3. X-ray crystal structure determination of **1**·0.5Et_2O

Suitable crystals of **1**·0.5Et_2O for X-ray analysis were obtained as described above. The intensity data were collected at 173(2) K on a Kappa CCD diffractometer[2] with graphite-monochromated Mo-Kα radiation (λ = 0.71073 Å). Crystallographic and experimental details are given in Table S1. The structure was solved by direct methods (SHELXS-97) and refined by full-matrix least-squares procedures (based on F^2, SHELXL-97)[3] with anisotropic thermal parameters for all the non-hydrogen atoms. All H atoms were placed into the geometrically calculated positions (SHELXL-97 procedures) and refined by using a riding model. A MULTISCAN absorption correction was used.[4] The SQUEEZE[5] instruction was applied to eliminate some residual electron density assigned to

half a molecule of diethyl ether. CCDC 868530 contains the supplementary crystallographic data for this paper that can be obtained free of charge from the Cambridge Crystallographic Data Centre via www.ccdc.cam.ac.uk/data_request/cif.

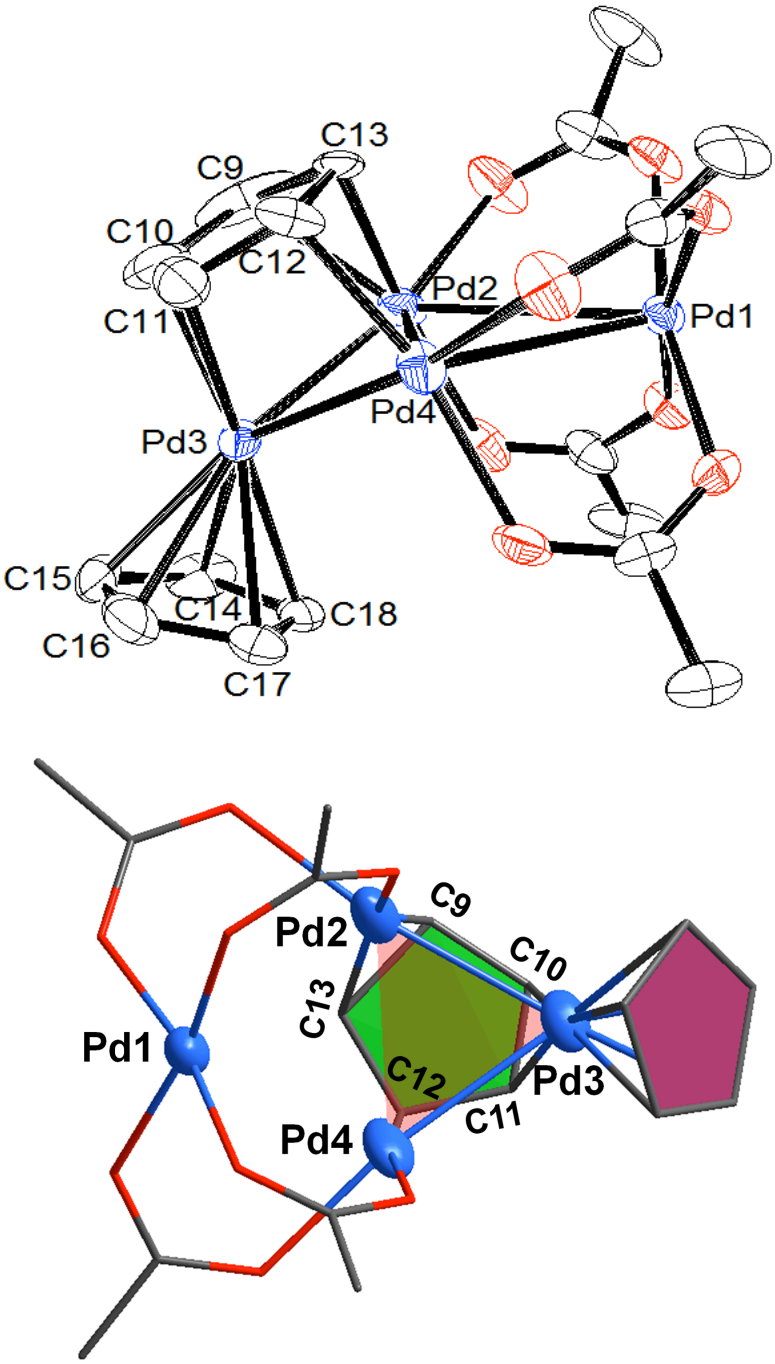

Figure S1. Top: ORTEP of the molecular structure of **1** in the crystal of **1**·0.5Et_2O (thermal ellipsoids are given at the 30% probability level; hydrogen atoms are omitted for clarity). Bottom: a perspective view of the structure of **1**.

***Table S1**:* Crystal data and structure refinement details for **1**·0.5Et_2O.

Empirical formula	$C_{18}H_{22}O_8Pd_4$
Formula weight [g/mol]	791.96
Temperature [K]	173(2)
Crystal colour	black
Crystal size [mm^3]	0.08×0.12×0.22
Crystal system	monoclinic
Space group	*C*2/*c*
a [Å]	30.142(4)
b [Å]	8.6063(10)
c [Å]	18.248(2)
β [º]	90.703(3)
V [$Å^3$]	4733.5(10)
Z	8
D_{calc} (g/cm^3)	2.223
μ (Mo Kα) (mm^{-1})	3.029
F(000)	3024
Reflections collected	15929
Independent reflections	5715
Observed refl. [$I > 2\sigma(I)$]	3531
Data/restraints/parameters	6390/0/275
Goodness-of-fit (S) on F^2	1.064
Final *R* indices [$I > 2\sigma(I)$]	$R1 = 0.0674$, $wR_2 = 0.1518$
R indices (all data)	$R1 = 0.1125$, $wR_2 = 0.1693$
Largest diff. peak and hole [e $Å^{-3}$]	1.594/ –1.557

4. References

(1) (a) P. Braunstein, R. Bender and J.-M. Jud, *Inorg. Synth*. 1989, **26**, 341. (b) T. K. Panda, M. T. Gamer and P. W. Roesky, *Organometallics*, 2003, **22**, 877.

(2) Bruker-Nonius *Kappa CCD Reference Manual*; Nonius BV, Delft, The Netherlands, 1998.

(3) G. M. Sheldrick, *Acta Cryst.* 2008, **A64**, 112.

(4) R. H. Blessing, *Acta Crystallogr., Sect A* 1995, **51**, 33.

(5) P. van der Sluis and A. L. Spek, *Acta Cryst.* 1990, **A46**, 194.

II. Computational Section

1. Computational details: methods and theory

Relativistic density functional theory (DFT) calculations were performed using the Amsterdam Density Functional (ADF) program developed by Baerends and others.[1,2] The numerical integration was performed using the procedure developed by te Velde *et al.*[2g,h] The MOs were expanded in a large uncontracted set of Slater type orbitals (STOs): TZ2P (no Gaussian functions are involved).[2i] The TZ2P basis set of triple-ζ quality (Basis Set System I) was used for all atoms and augmented with two sets of polarisation functions, i.e. 2*p* and 3*d* on H, 3*d* and 4*f* on C and O, 5*p* and 4*f* on Pd. An auxiliary set of *s*, *p*, *d*, *f* and *g* STOs was used to fit the molecular density and to represent the Coulomb and exchange potentials accurately in each self-consistent field cycle.[2j] Equilibrium structures were optimised in the gas phase using analytical gradient techniques.[2k] The core shells of C (1*s*), O (1*s*), and Pd (up to 3*d)* were treated by the frozen-core approximation.[2c] Grimme's dispersion corrections of D-[3a] and D3-generation[3b] for the DFT functionals were implemented. Energy minima in the gas phase were verified to be equilibrium structures through vibrational analysis.[4] The minima were found to have zero imaginary frequencies. Scalar relativistic effects were accounted for using the zeroth-order regular approximation (ZORA).[5]

In order to estimate the accuracy and sensitivity of the applied DFT methods, geometry optimisations were performed with the exchange-correlation (XC) energy functionals such as LDA, GGA (BP86, PBE, OPBE) and hybrid B3LYP as well as with HF (see Table S2).

Bond Analysis

To gain a deeper insight into the stability and nature of the internal interactions and bonding in $\mathbf{1}_{\mathbf{comput}}$ and $\mathbf{2}_{\mathbf{comput}}$, their energy decomposition analyses (EDA) were carried out.[6-8] In the EDA, the total binding energy ΔE associated with the formation of a molecular structure from smaller molecular fragments, A and B, is in general made up of two major components (eq. 1):

$$\Delta E = \Delta E_{def} + \Delta E_{int} \qquad (1)$$

In this formula, the deformation (or preparation) energy ΔE_{def} is the energy required to deform two individual (isolated) fragments A and B from their equilibrium structure to the geometry that they acquire in the overall molecule. The interaction energy ΔE_{int} corresponds to the actual energy change when these geometrically distorted fragments are combined to form the final structure. It is analysed in the framework of the Kohn-Sham Molecular Orbital (MO) model,[6-9] using a quantitative decomposition into electrostatic interaction, Pauli repulsion (or exchange repulsion or overlap repulsion), and (attractive) orbital interactions (eq. 2):[6]

$$\Delta E_{int} = \Delta V_{elstat} + \Delta E_{Pauli} + \Delta E_{oi} \qquad (2)$$

The term ΔV_{elstat} corresponds to the classical electrostatic interaction between the unperturbed charge distributions ρ_A and ρ_B of the prepared (*i.e*. distorted) fragments that adopt their positions in the overall molecule, and is usually attractive. The Pauli repulsion term, ΔE_{Pauli}, comprises the destabilizing interactions between occupied orbitals and is responsible for the steric repulsion. This repulsion is caused by the fact that two electrons with the same spin cannot occupy the same region in space. Its energy corresponds to the transition from the superposition of the unperturbed electron densities $\rho_A + \rho_B$ of the geometrically distorted fragments to the wavefunction $\psi^0 = N \hat{A} [\psi_A \cdot \psi_B]$, that properly obeys the Pauli principle through explicit antisymmetrisation ($\hat{A}$ operator) and renormalisation (N constant) of the product of fragment wavefunctions. The orbital interaction ΔE_{oi} in any MO model, and therefore also in Kohn-Sham theory, accounts for electron-pair bonding,[6] charge transfer (*i.e*. donor–acceptor interactions between occupied orbitals on one moiety with unoccupied orbitals of the other, including the HOMO–LUMO interactions) and polarisation (empty–occupied orbital mixing on one fragment due to the presence of another fragment).

The orbital interaction energy can be decomposed into the contributions from each irreducible representation Γ of the interacting system (eq. 3) using the extended transition state (ETS) scheme developed by Ziegler and Rauk[7] (note that this approach differs in this respect from the Morokuma scheme,[8] which instead attempts a decomposition of the orbital interactions into polarisation and charge transfer):

$$\Delta E_{\text{oi}} = \Sigma_\Gamma \Delta E_\Gamma \qquad (3)$$

Charge Analysis

The electron density distribution was analysed using the Voronoi deformation density (VDD) method[10] and the Hirshfeld scheme[11] for computing atomic charges. The VDD atomic charge Q_A^{VDD} was computed as the (numerical) integral[2a,g,h] of the deformation density $\Delta\rho(\mathbf{r}) = \rho(\mathbf{r}) - \Sigma_B \rho_B(\mathbf{r})$ in the volume of the Voronoi cell of atom A (Eq. 4). The VDD method is based on the partitioning of space into non-overlapping atomic areas modeled as Voronoi cells and then computing the deformation density within those cells (*i.e*. the extent to which electron density differs from that of an unbonded atom) (cf. the Wigner-Seitz cells in crystals[10c]). For an atom A, it is defined as:

$$Q_A^{\text{VDD}} = -\int_{\substack{\text{Voronoi} \\ \text{cell of A}}} \left(\rho(\mathbf{r}) - \sum_B \rho_B(\mathbf{r})\right) d\mathbf{r} \qquad (4)$$

Here, $\rho(\mathbf{r})$ is the electron density of the molecule and $\Sigma_B\ \rho_B(\mathbf{r})$ the superposition of atomic densities ρ_B of a fictitious promolecule without chemical interactions that is associated with the situation in which all atoms are neutral. The interpretation of the VDD charge Q_A^{VDD} is rather straightforward and transparent. Instead of measuring the amount of charge associated with a particular atom A, Q_A^{VDD} directly monitors how much charge flows, due to chemical interactions, out of ($Q_A^{VDD} > 0$) or into ($Q_A^{VDD} < 0$) the Voronoi cell of atom A, that is, the region of space that is closer to nucleus A than to any other nucleus.

Electron Localisation Function (ELF) Analysis

In order to obtain ELF functions, the single point (SP) calculations were first performed with the Gaussian 09 program[12] at the PBE level in combination with the Stuttgart RSC 1997 (SDD) RECP for the Pd atoms and the triple split-valence basis sets 6-311+G(d,p) for the H, C, O and P atoms (Basis Set System II).[13] The SP calculations were carried out on the experimental geometry of **1** as well as the equilibrium geometries of $\mathbf{1}_{\mathbf{comput}}$ and $\mathbf{2}_{\mathbf{comput}}$ obtained at ZORA-PBE-D3/TZ2P using the ADF program. Then, ELF functions were computed from the wave functions issued from the Gaussian 09 program using the DGRID program package of Kohout.[14] The possibility offered by the DGRID program to integrate the electronic density in the ELF basins gives access to accurate chemical information such as bond order or ligand field effect on metal ion valence shells. A precise description of the ELF function and examples were published by Piquemal *et al*.[15]

Natural Bond Orbital (NBO) Analysis

NBO analysis of $\mathbf{1}_{\mathbf{comput}}$ was performed with NBO Version 3.1[16] incorporated in the Gaussian 09 program.[12] The triple-zeta-valence basis set (def2-TZVP,[17] Basis Set System III) was employed in the PBE calculations and used for all atoms.

2. Results of the computational studies

To better understand the electronic structure of the unusual cluster **1**, relativistic dispersion–(non)-corrected density functional calculations were applied. Firstly, gas-phase calculations were conducted on the DFT-optimised structures of complex **1** for its different spin multiplicities S = 0 (singlet), 1 (triplet), and 2 (quintet). We established that the ground state is a singlet (S = 0) referred to as $\mathbf{1}_{\mathbf{comput}}$ and the other spin states are too high in energy to compete with the S = 0 state. Inclusion of dispersion effects in the structure optimisations only slightly affects the ground state equilibrium structure, $\mathbf{1}_{\mathbf{comput}}$, but provides a better agreement with the experimental geometry of **1** (Table S2). Because the PBE density functional has been shown to be one of the three best GGA-DFT functionals (along with BP86 and PW91), producing the most accurate optimised geometries using the ADF program package,[18] geometries and energies were further calculated at the PBE level of the generalised gradient approximation (GGA) and augmented with the Grimme's dispersion correction of D3 generation.[3] Thus, the contribution of the dispersion term to the total bonding energy, ΔE_{total}, of $\mathbf{1}_{\mathbf{comput}}$ is relatively small, only 0.45%. It arises mostly from the $Pd_3(OAc)_4$ subunit of **1**, since the contribution of dispersion effects in the related optimised structure of the complex $[Pd_3(\mu\text{-}OAc)_6]$ was found to be 0.39% of ΔE_{total}.

Table S2: Comparison between the structural parameters of the experimental geometry of **1** and its DFT optimised geometries.

Parameter	Exptl.	ZORA-*Functional*/TZ2P									
		HF	LDA	BP86	BP86-D3	OPBE	PBE	PBE-D	PBE-D3	B3LYP	B3LYP-D3
Pd(1)–Pd(2)	3.099	3.350	2.927	3.038	3.014	3.005	3.035	3.076	3.022	3.148	3.115
Pd(1)–Pd(4)	3.046	3.347	2.979	3.114	3.079	3.077	3.104	3.138	3.093	3.212	3.195
Pd(2)–Pd(4)	2.747	2.957	2.736	2.796	2.816	2.731	2.799	2.843	2.806	2.832	2.849
Pd(2)–Pd(3)	2.587	2.591	2.581	2.664	2.616	2.639	2.654	2.617	2.631	2.615	2.582
Pd(3)–Pd(4)	2.588	2.749	2.586	2.667	2.635	2.648	2.662	2.634	2.645	2.632	2.602
Pd(2)–η^2-Cp$^{\mu3}$	2.175,	2.247,	2.131,	2.180,	2.186,	2.114,	2.173,	2.130,	2.176,	2.202,	2.211,
	2.323	2.365	2.151	2.200	2.210	2.129	2.192	2.151,	2.197	2.246	2.260
Pd(3)–η^2-Cp$^{\mu3}$	2.108,	2.265,	2.086,	2.140,	2.133,	2.079,	2.130,	2.181,	2.128,	2.160,	2.156,
	2.196	2.283	2.094	2.150	2.158	2.082,	2.141	2.204,	2.143	2.225	2.233
Pd(4)–η^1-Cp$^{\mu3}$	2.057	2.034	2.003	2.045	2.042	1.992	2.040	2.041	2.038	2.059	2.059
$Z_{Pd2,Pd3,Pd4}$–$Z_{\mu3\text{-}Cp}$	2.011	2.093	1.967	2.012	2.015	1.950	2.004	2.009	2.006	2.045	2.049
Pd(3)–η^5-Cp	2.196,	2.262,	2.173,	2.237,	2.221,	2.205,	2.233,	2.204,	2.227,	2.250,	2.233,
	2.250,	2.420,	2.235,	2.306,	2.298,	2.252,	2.299,	2.274,	2.295,	2.321,	2.313,
	2.265,	2.422,	2.256,	2.337,	2.317,	2.279,	2.326,	2.298,	2.319,	2.347,	2.329,
	2.297,	2.570,	2.329,	2.415,	2.409,	2.322,	2.401,	2.387,	2.397,	2.410,	2.407,
	2.297	2.579	2.336	2.432	2.420	2.333	2.415	2.400	2.410	2.427	2.420
Pd(3)–$Z_{Cp}^{\eta5}$	1.918	2.140	1.919	2.007	1.992	1.931	1.995	1.969	1.989	2.018	2.005

Table S3: Mulliken orbital populations of the Pd centres obtained from the ZORA-PBE-D3/TZ2P computations using the experimental geometry of **1**,[a] and the optimised geometries of $\mathbf{1}_{\mathbf{comput}}$ and $\mathbf{2}_{\mathbf{comput}}$.

Geometry	Pd centre	s	d	p
1	Pd(1)	0.22	8.52	0.34
	Pd(2)	0.25	8.82	0.46
	Pd(3)	0.33	8.74	0.66
	Pd(4)	0.22	8.81	0.38
$\mathbf{1}_{\mathbf{comput}}$ [b]	Pd(1)	0.22	8.53	0.33
	Pd(2)	0.25	8.72	0.49
	Pd(3)	0.33	8.76	0.67
	Pd(4)	0.22	8.80	0.35
$\mathbf{2}_{\mathbf{comput}}$	Pd(1)	0.31	8.98	0.46
	Pd(2)	0.31	8.98	0.46

[a] Calculated using the x,y,z-coordinates from X-ray crystallography of **1**·0.5Et_2O. [b] Natural electron configurations of the Pd centres obtained from NBO analysis of $\mathbf{1}_{\mathbf{comput}}$ at PBE/def2-TZVP are the following: Pd(1) $5s^{0.31}4d^{8.72}5p^{0.29}$, Pd(2) $5s^{0.30}4d^{8.95}5p^{0.40}$, Pd(3) $5s^{0.30}4d^{9.05}5p^{0.58}$, Pd(4) $5s^{0.29}4d^{9.06}5p^{0.30}$.

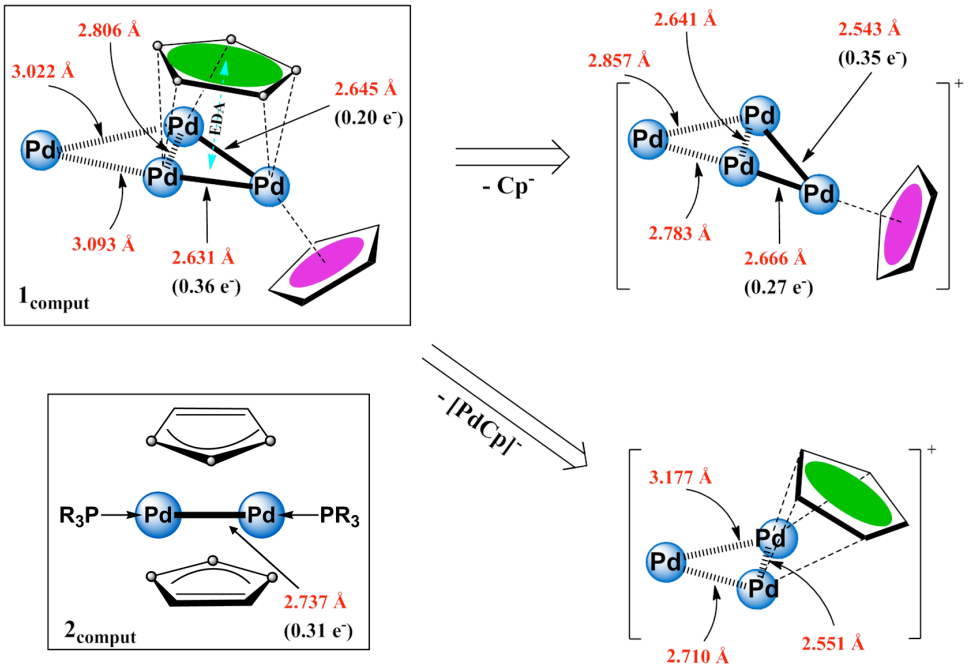

Scheme S1. Structural representations of $\mathbf{1}_{comput}$, its cationic fragments, and $\mathbf{2}_{comput}$ (R = Me). The carboxylate bridges are omitted for clarity. The values of the Pd–Pd distances optimised at ZORA-PBE-D3/TZ2P are shown and the magnitudes of their ELF valence basins are given in parentheses.

Mayer bond orders. The Pd(2)–Pd(3) and Pd(3)–Pd(4) interactions in **1**$_{\mathbf{comput}}$ have Mayer bond orders[19] (MBOs) of 0.577 and 0.458, respectively, whereas the MBOs for Pd(1)–Pd(2), Pd(1)–Pd(4) and Pd(2)–Pd(4) are 0.156, 0.145 and 0.248, respectively. The values of the MBOs computed for the Pd–Pd interactions in **1** are the following: 0.125 for Pd(1)–Pd(2), 0.147 for Pd(1)–Pd(4), 0.285 for Pd(2)–Pd(4), 0.600 for Pd(2)–Pd(3) and 0.545 for Pd(3)–Pd(4). The Mayer bond order for Pd(1)–Pd(2) in **2**$_{\mathbf{comput}}$ is 0.479.

Table S4: Population of the ELF valence basins (in e) for the Pd–Pd bonds in **1** and **1**$_{\mathbf{comput}}$.

Geometry	Pd(2)–Pd(3)	Pd(3)–Pd(4)
1	0.32	0.28
1$_{\mathbf{comput}}$	0.36	0.20

Table S5: Relevant absolute chemical shifts (in ppm) computed for **1** and **1**$_{\mathbf{comput}}$ at ZORA-PBE-D3/TZ2P. The NICS values[a] are given as well.

Geometry	Pd(1)	Pd(2)	Pd(3)	Pd(4)	NICS-1	NICS-2
1[b]	–2319	–758	+2411	–806	+12	–45
1$_{\mathbf{comput}}$	–2569	–300	+2463	–679	+10	–44

[a] Nucleus independent chemical shifts (NICS) computed at the geometrical centre of Pd(1),Pd(2),Pd(4) triangle (NICS-1) from the carboxylate subfragment and at the geometrical centre of Pd(2),Pd(3),Pd(4) triangle (NICS-2) bonded to μ_3-Cp. [b] Calculated using the x,y,z-coordinates from X-ray crystallography of **1**·0.5Et_2O.

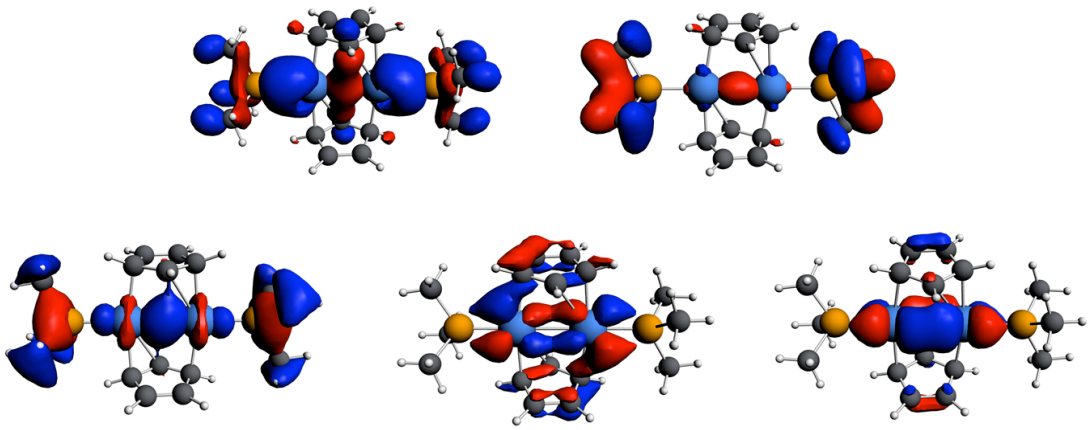

Figure S2. Spatial representation of the Boys-Foster localised orbitals[20] (±0.03 isosurface value) between two Pd atoms of complex **2**$_{\mathbf{comput}}$.

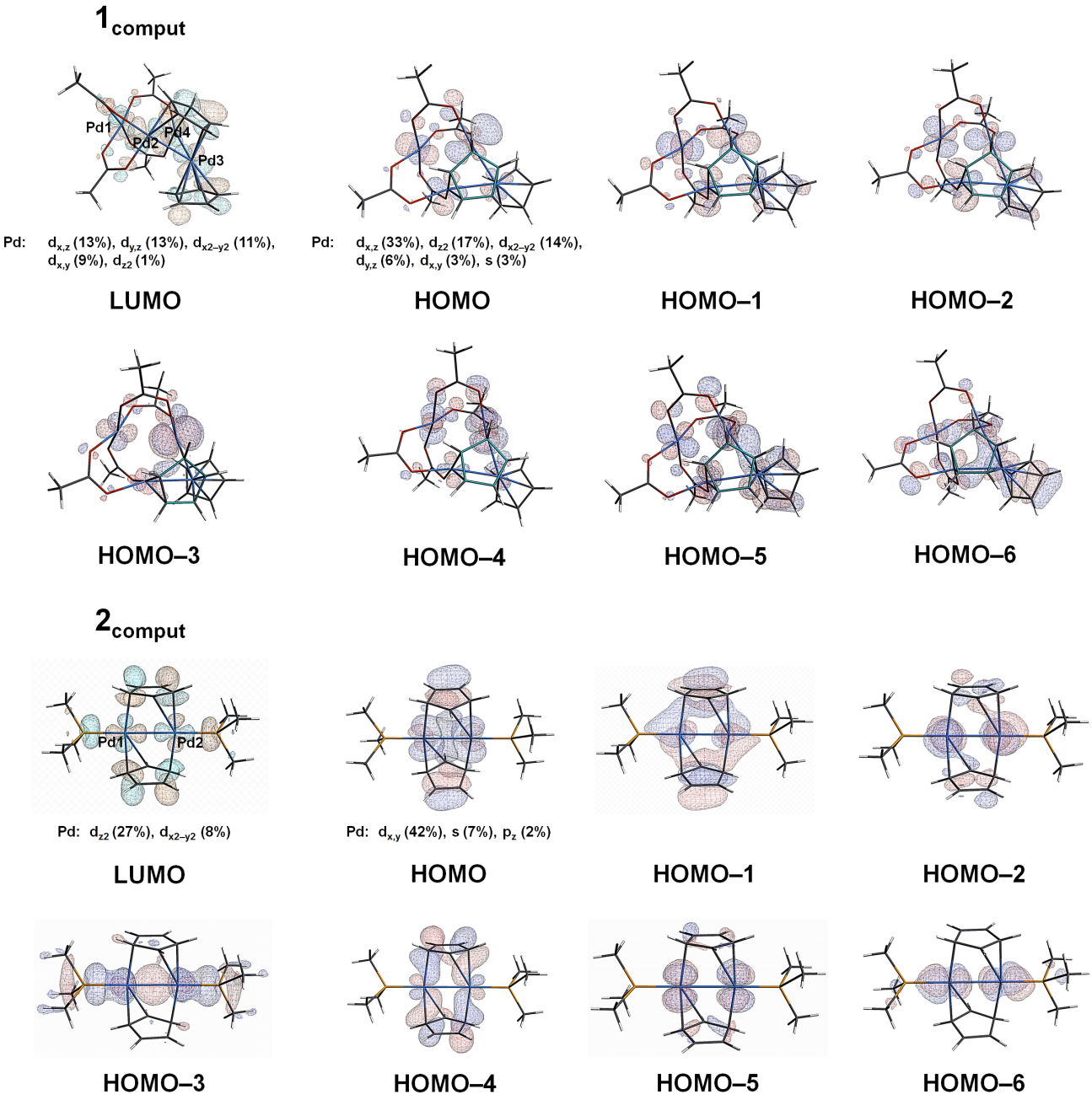

Figure S3. Spatial representation of the most relevant frontier molecular orbitals (±0.03 isosurface value) of complexes $\mathbf{1}_{\mathbf{comput}}$ (top) and $\mathbf{2}_{\mathbf{comput}}$ (below). $\mathbf{2}_{\mathbf{comput}}$ exhibits a relatively large HOMO–LUMO gap of 2.22 eV indicative of enhanced kinetic stability compared to $\mathbf{1}_{\mathbf{comput}}$ for which the HOMO–LUMO gap is 1.12 eV, and to $[Pd_3(OAc)_6]$ with a HOMO–LUMO gap of 1.44 eV.

Energy Decomposition Analysis (EDA). In order to gain further insight into the metal-metal and metal-Cp interactions in **1** and **1**$_{\mathbf{comput}}$, three models involving different fragments (*i*) $[Pd_3(\mu\text{-}OAc)_4Pd(\eta^5\text{-}Cp)]^+$ and Cp^- (model A), (*ii*) $[Pd_3(\mu\text{-}OAc)_4(\mu_2\text{-}Cp)]^+$ and $PdCp^-$ (model B) and (*iii*) $[Pd_3(\mu\text{-}OAc)_4]$ and $PdCp_2$ (model C) were subjected to the EDA[6-8] (Figure S4). In the case of **2**$_{\mathbf{comput}}$, we studied the interaction between $[Pd_2(PMe_3)_2]^{2+}$ and two μ_2-Cp^- units. The results illustrated in Tables S6 and S7 show that the electrostatic attractions, ΔV_{elstat}, dominate in all models and are in the range 57–68% of the bonding interactions, *i.e.* $\Delta V_{elstat} + \Delta E_{oi}$. However, it is noteworthy that the orbital terms ranging accordingly from 32 to 43% significantly contribute to the attractive interactions. Even though strong Pauli repulsion, ΔE_{Pauli}, arises between the all interacting fragments considered for **1**$_{\mathbf{comput}}$ and **2**$_{\mathbf{comput}}$, the strongly attractive electrostatic forces, ΔV_{elstat}, outweigh quantum mechanical ones,[21] *i.e.* $\Delta E_{oi} + \Delta E_{Pauli}$ where the Pauli repulsion term represents the electron pair repulsion. Other attractive forces present in the analysed interactions are the dispersion energy terms (ΔE_{disp}), however they are too small to be taken into consideration (1–2% of the bonding interactions, *i.e.* $\Delta V_{elstat} + \Delta E_{oi} + \Delta E_{disp}$). Thus, the EDA suggests that the attractive ΔV_{elstat} terms are the ones which *mostly* stabilise the bonding interactions between the fragments analysed for **2**$_{\mathbf{comput}}$ as well as in models A, B and C for **1** and **1**$_{\mathbf{comput}}$. The bond dissociation energies (BDEs), D_e, calculated for **1**$_{\mathbf{comput}}$ in models A, B and C show the same trend as the interaction energies, ΔE_{int}, *i.e.* their absolute values decrease on going from model A to C. The BDEs show that the interactions between the ionic fragments in models A and B are approximately two times stronger than the interaction between the neutral fragments, $[Pd_3(\mu\text{-}OAc)_4]$ (optimised within the C_{2v} symmetry; NIMAG =1, B1: *i*25 cm^{-1}) and $Pd^{II}(\eta^3\text{-}Cp)_2$, in model C. In addition, combining the latter into a single molecule, **1**$_{\mathbf{comput}}$, is an exothermic process in all models A, B and C, as illustrated in Figure S4 (see ΔE_{rel}).

Table S6: Energy decomposition analysis ($kcal \cdot mol^{-1}$) of the interactions between $[Pd_3(\mu\text{-}OAc)_4Pd(\eta^5\text{-}Cp)]^+$ and Cp^- in model A, $[Pd_3(\mu\text{-}OAc)_4(\mu_2\text{-}Cp)]^+$ and $PdCp^-$ in model B and $[Pd_3(\mu\text{-}OAc)_4]$ and $PdCp_2$ in model C for **1**$_{\mathbf{comput}}$ and of the interactions between the two Cp^- ligands and the $[Pd_2(PMe_3)_2]^{2+}$ unit for **2**$_{\mathbf{comput}}$. The EDA is performed at ZORA-PBE-D3/TZ2P.

Complex	ΔE_{int}[a]	ΔE_{Pauli}	ΔV_{elstat}	ΔE_{oi}	ΔE_{disp}	ΔE_{def}	D_e[b]
1$_{\mathbf{comput}}$ (A)	–247.6	520.0	–499.2 (65.6%)	–261.4 (34.4%)	–7.0	41.8	205.8
1$_{\mathbf{comput}}$ (B)	–235.0	322.0	–346.8 (63.2%)	–201.8 (36.8%)	–8.4	38.9	196.1
1$_{\mathbf{comput}}$ (C)	–160.5	434.8	–340.8 (58.4 %)	–243.1 (41.6 %)	–11.5	52.1	108.4
2$_{\mathbf{comput}}$	–529.6	443.2	–652.6 (67.8%)	–309.3 (32.2%)	–10.9		

[a] $\Delta E_{int} = \Delta V_{elstat} + \Delta E_{Pauli} + \Delta E_{oi} + \Delta E_{disp}$. [b] ΔE (= $-D_e$) = $\Delta E_{int} + \Delta E_{def}$.

Table S7: Energy decomposition analysis (kcal·mol^{-1}) of the interactions between $Pd_3(\mu\text{-}OAc)_4Pd(\eta^5\text{-}Cp)]^+$ and Cp^- in model A, $[Pd_3(\mu\text{-}OAc)_4(\mu_2\text{-}Cp)]^+$ and $PdCp^-$ in model B and $[Pd_3(\mu\text{-}OAc)_4]$ and $PdCp_2$ in model C for **1**. The EDA is performed at ZORA-PBE-D3/TZ2P.

Complex	ΔE_{int}[a]	ΔE_{Pauli}	ΔV_{elstat}	ΔE_{oi}	ΔE_{disp}
1[b] (A)	–203.6	484.3	–455.3 (66.9%)	–225.1 (33.1%)	–7.4
1[b] (B)	–222.6	368.7	–372.8 (64.0 %)	–209.8 (36.0 %)	–8.8
1[b] (C)	–119.0	423.5	–306.8 (57.8 %)	–224.3 (42.2 %)	–11.4

[a] $\Delta E_{int} = \Delta V_{elstat} + \Delta E_{Pauli} + \Delta E_{oi} + \Delta E_{disp}$. [b] Calculated using the x,y,z-coordinates from X-ray crystallography of **1**·0.5Et_2O.

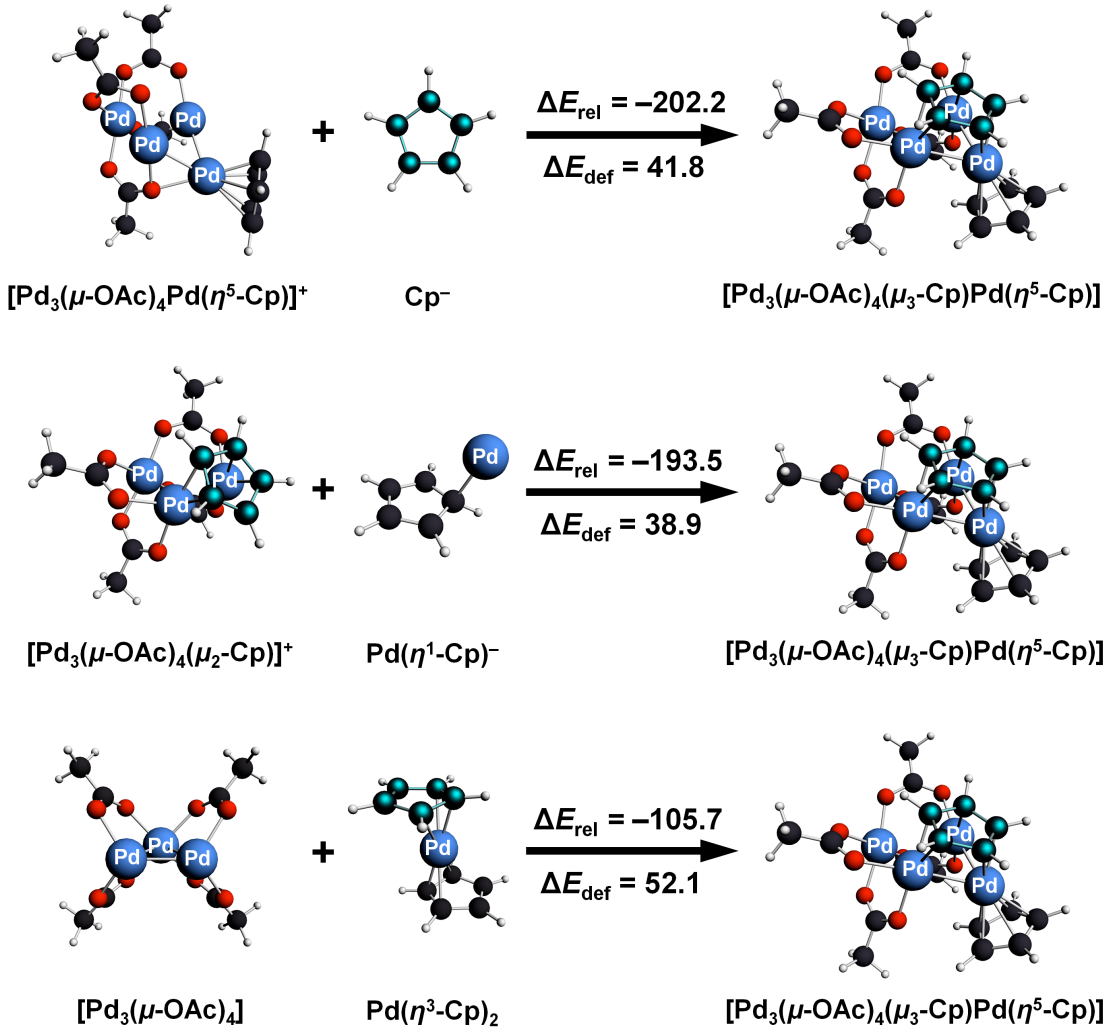

Figure S4. Representation of the theoretically analysed association processes leading to the neutral structure $\mathbf{1}_{comput}$ from (*i*) the ionic fragments $[Pd_3(OAc)_4Pd(\eta^5\text{-}Cp)]^+$ and Cp^- in model A (top) and $[Pd_3(OAc)_4(\mu_2\text{-}Cp)]^+$ and $Pd^0(\eta^1\text{-}Cp)^-$ in model B (middle) and (*ii*) from the neutral fragments $[Pd_3(\mu\text{-}OAc)_4]$ and $Pd^{II}(\eta^3\text{-}Cp)_2$ in model C (bottom). Relative energies, ΔE_{rel} (incl. zero-point energy correction) and deformation energies, ΔE_{def} (the energy difference between the equilibrium structures of isolated ionic or neutral fragments, and the geometries that these fragments acquire in the equilibrium structure $\mathbf{1}_{comput}$), are shown in kcal·mol^{-1}.

3. References

(1) ADF2010.01, SCM, Theoretical Chemistry, Vrije Universiteit, Amsterdam, The Netherlands, http://www.scm.com. E. J. Baerends, J. Autschbach, A. Bérces, C. Bo, P. M. Boerrigter, L. Cavallo, D. P. Chong, L. Deng, R. M. Dickson, D. E. Ellis, L. Fan, T. H. Fischer, C. Fonseca Guerra, S. J. A. van Gisbergen, J. A. Groeneveld, O. V. Gritsenko, M. Grüning, F. E. Harris, P. van den Hoek, H. Jacobsen, G. van Kessel, F. Kootstra, E. van Lenthe, D. A. McCormack, V. P. Osinga, S. Patchkovskii, P. H. T. Philipsen, D. Post, C. C. Pye, W. Ravenek, P. Ros, P. R. T. Schipper, G. Schreckenbach, J. G. Snijders, M. Solà, M. Swart, D. Swerhone, G. te Velde, P. Vernooijs, L. Versluis, O. Visser, E. van Wezenbeek, G. Wiesenekker, S. K. Wolff, T. K. Woo and T. Ziegler.

(2) (a) G. te Velde, F. M. Bickelhaupt, E. J. Baerends, C. Fonseca Guerra, S. J. A. van Gisbergen, J. G. Snijders and T. Ziegler, *J. Comput. Chem.,* 2001, **22**, 931; (b) C. Fonseca Guerra, O. Visser, J. G. Snijders, G. te Velde and E. J. Baerends In *Methods and Techniques for Computational Chemistry*, (Eds.: E. Clementi, G. Corongiu), STEF: Cagliari, 1995, pp. 305–395; (c) E. J. Baerends, D. E. Ellis and P. Ros, *Chem. Phys.,* 1973, **2**, 41; (d) E. J. Baerends and P. Ros, *Chem. Phys.,* 1975, **8**, 412; (e) E. J. Baerends and P. Ros, *Int. J. Quantum Chem. Symp.,* 1978, **12**, 169; (f) C. Fonseca Guerra, J. G. Snijders, G. te Velde and E. J. Baerends, *Theor. Chem. Acc.,* 1998, **99**, 391; (g) P. M. Boerrigter, G. te Velde and E. J. Baerends, *Int. J. Quantum Chem.,* 1988, **33**, 87; (h) G. te Velde and E. J. Baerends, *J. Comp. Phys.,* 1992, **99**, 84; (i) J. G. Snijders, P. Vernooijs and E. J. Baerends, *At. Nucl. Data Tables,* 1981, **26**, 483; (j) J. Krijn and E. J. Baerends, *Fit-Functions in the HFS-Method; Internal Report (in Dutch)*, Vrije Universiteit, Amsterdam, 1984; (k) L. Versluis and T. Ziegler, *J. Chem. Phys.,* 1988, **88**, 322; (l) J. C. Slater, *Quantum Theory of Molecules and Solids, Vol. 4*, McGraw-Hill, New York, 1974; (m) A. D. Becke, *J. Chem. Phys.,* 1986, **84**, 4524; (n) A. D. Becke, *Phys. Rev. A,* 1988, **38**, 3098; (o) S. H. Vosko, L. Wilk and M. Nusair, *Can. J. Phys.,* 1980, **58**, 1200; (p) J. P. Perdew, *Phys. Rev. B,* 1986, **33**, 8822 (Erratum: *Phys. Rev. B,* 1986, **34**, 7406); (q) L. Fan and T. Ziegler, *J. Chem. Phys.,* 1991, **94**, 6057.

(3) (a) S. Grimme, *J. Comput. Chem.,* 2006, **27**, 1787; (b) S. Grimme, J. Antony, S. Ehrlich and H. Krieg, *J. Chem. Phys.,* 2010, **132**, 154104.

(4) (a) A. Bérces, R. M. Dickson, L. Fan, H. Jacobsen, D. Swerhone and T. Ziegler, *Comput. Phys. Commun.,* 1997, **100**, 247; (b) H. Jacobsen, A. Bérces, D.

Swerhone and T. Ziegler, *Comput. Phys. Commun.,* 1997, **100**, 263; (c) S. K. Wolff, *Int. J. Quantum Chem.,* 2005, **104**, 645.

(5) E. van Lenthe, E. J. Baerends and J. G. Snijders, *J. Chem. Phys*., 1994, **101**, 9783.

(6) (a) F. M. Bickelhaupt and E. J. Baerends, In *Reviews in Computational Chemistry*; K. B. Lipkowitz and D. B. Boyd, Eds.; Wiley-VCH: New York, 2000; **15**, p. 1; (b) F. M. Bickelhaupt, N. M. M. Nibbering, E. M. van Wezenbeek and E. J. Baerends, *J. Phys. Chem.,* 1992, **96**, 4864; (c) F. M. Bickelhaupt, A. Diefenbach, S. P. de Visser, L. J. de Koning and N. M. M. Nibbering, *J. Phys. Chem. A,* 1998, **102**, 9549.

(7) (a) T. Ziegler and A. Rauk, *Theor. Chim. Acta,* 1977, **46**, 1; (b) T. Ziegler and A. Rauk, *Inorg. Chem.,* 1979, **18**, 1558; (c) T. Ziegler and A. Rauk, *Inorg. Chem.,* 1979, **18**, 1755.

(8) (a) See also: K. Kitaura and K. Morokuma, *Int. J. Quantum Chem.,* 1976, **10**, 325; (b) K. Morokuma, *Acc. Chem. Res.,* 1977, **10**, 294.

(9) E. J. Baerends and O. V. Gritsenko, *J. Phys. Chem. A,* 1997, **101**, 5383.

(10) (a) F. M. Bickelhaupt, N. J. R. van Eikema Hommes, C. Fonseca Guerra and E. J. Baerends, *Organometallics,* 1996, **15**, 2923; See also: (b) C. Fonseca Guerra, J.-W. Handgraaf, E. J. Baerends and F. M. Bickelhaupt, *J. Comput. Chem.,* 2004, **25**, 189; Voronoi cells are equivalent to Wigner-Seitz cells in crystals; for the latter, see: (c) C. Kittel, *Introduction to Solid State Physics*; Wiley: New York, **1986**.

(11) F. L. Hirshfeld, *Theor. Chim. Acta,* 1977, **44**, 129.

(12) M. J. Frisch, G. W. Trucks, H. B. Schlegel, G. E. Scuseria, M. A. Robb, J. R. Cheeseman, G. Scalmani, V. Barone, B. Mennucci, G. A. Petersson, H. Nakatsuji, M. Caricato, X. Li, H. P. Hratchian, A. F. Izmaylov, J. Bloino, G. Zheng, J. L. Sonnenberg, M. Hada, M. Ehara, K. Toyota, R. Fukuda, J. Hasegawa, M. Ishida, T. Nakajima, Y. Honda, O. Kitao, H. Nakai, T. Vreven, J. A. Montgomery, Jr., J. E. Peralta, F. Ogliaro, M. Bearpark, J. J. Heyd, E. Brothers, K. N. Kudin, V. N. Staroverov, T. Keith, R. Kobayashi, J. Normand, K. Raghavachari, A. Rendell, J. C. Burant, S. S. Iyengar, J. Tomasi, M. Cossi, N. Rega, J. M. Millam, M. Klene, J. E. Knox, J. B. Cross, V. Bakken, C. Adamo, J. Jaramillo, R. Gomperts, R. E. Stratmann, O. Yazyev, A. J. Austin, R. Cammi, C. Pomelli, J. W. Ochterski, R. L. Martin, K. Morokuma, V. G. Zakrzewski, G. A. Voth, P. Salvador, J. J. Dannenberg, S. Dapprich, A. D. Daniels, O. Farkas, J. B. Foresman, J. V. Ortiz, J. Cioslowski and D. J. Fox, Gaussian **09**, Revision B.01, Gaussian, Inc., Wallingford CT, 2010.

(13) For SDD, see: (a) M. Dolg, U. Wedig, H. Stoll and H. Preuß, *J. Chem. Phys.*, 1987, **86**, 866. (b) D. Andrae, U. Häußermann, M. Dolg, H. Stoll and H. Preuß, *Theor.*

Chim. Acta, 1990, **77**, 123. For 6-311+G(d,p), see: (c) R. Krishnan, J. S. Binkley, R. Seeger and J. A. Pople, *J. Chem. Phys.,* 1980, **72**, 650. (d) K. Raghavachari and G. W. Trucks, *J. Chem. Phys.* 1989, **91**, 1062.

(14) M. Kohout, DGrid, version **4.5**, Radebeul, 2009.

(15) J.-P. Piquemal, J. Pilme, O. Parisel, H. Gerard, I. Fourre, J. Berges, C. Gourlaouen, A. De La Lande, M.-C. Van Severen and B. Silvi, *Intl. J. Quant. Chem.,* 2008, **108**, 1952.

(16) (a) Glendening, E. D.; Reed, A. E.; Carpenter, J. E.; Weinhold, F. NBO program, version 3.1. (b) Reed, A. E.; Curtiss, L. A.; Weinhold, F. *Chem. Rev.* **1988**, *88*, 899.

(17) F. Weigend and R. Ahlrichs, *Phys. Chem. Chem. Phys.,* 2005, **7**, 3297.

(18) M. Swart and J. G. Snijders, *Theor. Chem. Acc.,* 2003, **110**, 34. Erratum: *Theor. Chem. Acc.,* 2004, **111**, 56.

(19) I. Mayer, *Chem. Phys. Lett.,* 1983, **97**, 270.

(20) (a) C. Edmiston and K. Rudenberg, *Rev. Mod. Phys.,* 1963, **35**, 457; (b) J. M. Foster, S. F. Boys, *Rev. Mod. Phys.,* 1960, **32**, 300; (c) W. von Niessen, *J. Chem. Phys.,* 1972, **56**, 4290.

(21) A. Krapp, F. M. Bickelhaupt and G. Frenking, *Chem. Eur. J.,* 2006, **12**, 9196. According to their statement, "*A particular strength of the EDA is that it considers the total interatomic interactions that lead to the experimentally measurable bond dissociation energy and not only a particular fraction of the bond*".